Available online at www.sciencedirect.com
SCIENCE DIRECT®
Surface and Coatings Technology 179 (2004) 124–134
SURFACE & COATINGS TECHNOLOGY
www.elsevier.com/locate/surfcoat

Electroless nickel-plating on AZ91D magnesium alloy: effect of substrate microstructure and plating parameters

Rajan Ambat[a,*], W. Zhou[b]

[a]Metallurgy and Materials, School of Engineering, The University of Birmingham, Birmingham B15 2TT, UK
[b]School of Mechanical and Production Engineering, Nanyang Technological University, Singapore 639798, Singapore

Received 17 June 2002; accepted in revised form 14 July 2003

Abstract

Electroless nickel-plating on AZ91D magnesium alloy has been investigated to understand the effect of substrate microstructure and plating parameters. The initial stage of the deposition was investigated using scanning electron microscopy (SEM) and energy dispersive X-ray analysis on substrates plated for a very short interval of time. The early stage of growth was strongly influenced by the substrate microstructure. Plating was initiated on β-phase grains probably due to the galvanic coupling of β and eutectic α-phase. Once the β-phase was covered with the coating, it then spread onto eutectic α and primary α-phase. The coating produced with the optimised bath showed 7 wt.% phosphorus with a hardness of approximately 600–700 VHN. The optimum ligand to metal ion ratio was found to be 1:1.5, while the safe domain for thiourea (TU) was in the range of 0.5–1 mg/l. Fluoride was found to be an essential component of the bath to plate AZ91D alloy with an optimum value of 7.5 g/l. The presence of 0.25–0.5 mg/l mercapto-benzo-thiosole (MBT) found to accelerate the plating process.

Keywords: Magnesium alloy; Electroless nickel; Microstructure; Plating parameters

1. Introduction

Magnesium and its alloys, with one quarter of the density of steel and only two-thirds that of aluminium and a strength to weight ratio that far exceeds either of these, fulfill the role admirably as an 'ultra light weight' alloy. Hence, these alloys have obviously become the choice for weight reduction in portable microelectronics, telecommunications, aerospace and automobile applications etc.

The magnesium–aluminium system has been the basis of the most widely used magnesium alloys since these materials were introduced in Germany during the First World War. Most of these alloys contain 8–9% aluminium with small amounts of zinc [1,2].

A serious limitation for the potential use of several magnesium alloys and AZ91 in particular, is their susceptibility to corrosion. Magnesium alloys, especially those with high purity, have good resistance to atmospheric corrosion [3]. However, the addition of alloying elements modifies the corrosion behaviour in such a way that it can be beneficial or deleterious. The standard electrochemical potential of magnesium is -2.4 V vs. NHE, even though in aqueous solutions magnesium shows a potential of -1.5 V due to the formation of $Mg(OH)_2$ film [4]. Consequently, magnesium dissolves rapidly in aqueous solutions by evolving hydrogen below pH 11.0, the equilibrium pH value for $Mg(OH)_2$ [4].

Although the addition of several alloying elements such as aluminium, zinc and rare earths have been reported [5–12] to improve the corrosion resistance, technologically that does not satisfy the requirement for several applications. Hence, the application of a surface engineering technique is the most appropriate method to further enhance the corrosion resistance. Among the various surface engineering techniques that are available for this purpose, coating by electroless nickel is of special interest especially in the electronic industry, due to its conductivity and several other engineering prop-

*Corresponding author. Tel.: +44-121-414-5217; fax: +44-121-414-5232.
E-mail address: R.Ambat@bham.ac.uk (R. Ambat).

0257-8972/04/$ - see front matter © 2003 Elsevier B.V. All rights reserved.
doi:10.1016/S0257-8972(03)00866-1

Table 1
Chemical composition of the AZ91D alloy (in wt.%)

Al	Mn	Ni	Cu	Zn	Ca	Si	K	Fe	Mg
9.1	0.17	0.001	0.001	0.64	<0.01	<0.01	<0.01	<0.001	Bal

erties. Electroless nickel is well known for its corrosion resistance and hardness [13–18]. However, the nickel/Mg system is a classical example of cathodic coating on an anodic substrate. Hence, the porosity in the coating might influence the corrosion behaviour and service lifetime of the electroless nickel-plated magnesium. The protective ability of electroless nickel on many engineering materials is limited by the porosity in the coating [19–26].

Being a highly active metal, electroless plating of magnesium alloy needs special bath formulations and pre-cleaning treatments. Hence, the direct plating of magnesium is still a challenge for the researchers. The process becomes more complicated on AZ91 alloy due to the microstructural heterogeneity owing to the unequal distribution of aluminium within the three constituent phases namely primary α, eutectic α and β phases [26]. Therefore, the substrate material is electrochemically heterogeneous and each constituent behaves differently to the plating bath. The available information on electroless nickel-plating of magnesium alloys is very limited. This paper reports the work carried out on electroless nickel-coating of AZ91D magnesium alloy, more specifically, the effect of substrate microstructure on coating nucleation and the effect of various bath parameters.

2. Experimental

The substrate material used for the present investigation was AZ91D ingot-cast alloy. The chemical composition of the alloy is given in Table 1. Rectangular coupons of size $20\times40\times4$ mm were used for the investigation. The surface of the substrate material was wet-ground (using water) on 1000 grade SiC paper and polished on a diamond wheel using 6-μm diamond paste. The polished specimens were thoroughly washed with water before passing through the pre-cleaning schedule as shown in Table 2. The initial weight and dimensions of the specimens were measured prior to pre-cleaning steps. Immediately after the fluoride activation (last step in the pre-cleaning process), the specimen was quickly transferred to the coating bath (500 ml) in a glass container placed in a constant temperature water bath to maintain the required temperature. A fresh bath was used for each experiment to avoid any change in concentration of bath species. The bath composition and other parameters used in the present work are given in Table 3. The specimens were coated for the required length of time, removed from the bath, washed with water and acetone and air-dried. Final weight of the specimen was determined and the coating rate in μm/h was calculated from the weight gain. In this work, the initial weight of the specimen was measured prior to pre-cleaning steps. This is to avoid any surface oxidation due to time delay in transferring the substrate to the plating bath after fluoride activation step. However, to estimate the error in the weight gain calculation as a result of dissolution of substrate material during the pre-cleaning steps, a control experiment was carried out to measure the weight loss during the pre-cleaning process. The loss in weight during the pre-cleaning process was found to be insignificant, although the weight gain values reported were corrected for this weight loss. Duplicate experiments were conducted in each case, and the coating rate reported is the average of two experiments. The coated specimens were characterised to evaluate the coating performance. Coating morphology was analysed using optical (Axiolab ZEISS model) and scanning electron microscope (JEOL Model No.

Table 2
Optimised pre-cleaning steps

Ultrasonic degreasing using acetone
↓
Rinse in 10% NaOH at 60 °C for 5 min
↓
Water rinse
↓
6% chromic acid–5% nitric acid pickling for 45 s
↓
Water rinse
↓
Fluoride activation in HF (250 ml 70% HF/l) for 10 min
↓
Water rinse

Table 3
Optimised bath composition and coating parameters

Bath constituents and parameters	Quantity
Basic nickel carbonate ($NiCO_3$ $2Ni(OH)_2$ $4H_2O$)	9.7 g/l
Citric acid	5.2 g/l
Ammonium bifluoride	7.5 g/l
Hydrofluoric acid	11 ml/l
Thiourea (TU)	1 mg/l
Sodium hypophosphite	20 g/l
Ammonium hydroxide	To adjust pH
Temperature	80 °C
Agitation	Mild-mechanical

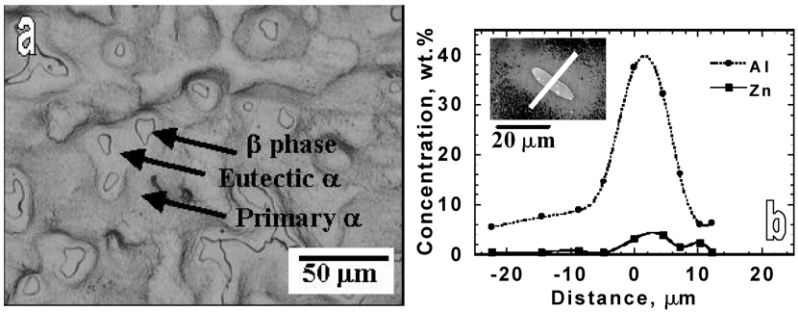

Fig. 1. AZ91 substrate: (a) microstructure and (b) Al and Zn concentration across the β-phase along the line shown in the picture.

5600LV). EDX analysis was used for the determination of phosphorus. Microhardness measurements were carried out using Shimadzu hardness testing machine (HMV 2000 model) using a load of 100 g. The structure of the deposit was determined using X-ray diffraction technique (Philips, Model No. PW1830).

For studying the coating nucleation, coupons were deposited for very short internals of time namely 1–5 min, and were analysed using SEM and EDX.

3. Results

3.1. Microstructure of substrate material

Fig. 1a shows microstructure of the substrate material AZ91D ingot. The microstructure consisted of primary α, eutectic α and β-phases (marked in the figure). β-phase is an intermetallic with the stoichiometric composition of $Mg_{17}Al_{12}$. Coring during solidification resulted in considerable variation in the distribution of aluminium and zinc in the microstructure of AZ91D alloy. Previously, we have reported the variation of aluminium and zinc concentration adjacent to β-phase in AZ91 ingot-cast alloy [26]. Fig. 1b gives a typical concentration profile of aluminium and zinc in AZ91D alloy along the line shown in the SEM picture (shown in the inset) measured using EDX. In general, the aluminium and zinc concentration at α regions near to β-phase (eutectic α) was high, which decreased with increase in distance from the β-phase [26]. The width of this aluminium rich region ($>8\%$) adjacent to the β-phase varied at different sites [26]. The concentration of aluminium typically varied between $\sim 35\%$ at the β-phase to approximately ~ 8–6% near or within the primary α-phase. This microstructural heterogeneity on the surface of the substrate complicates the process of electroless deposition.

3.2. Electroless nickel-coating

Fig. 2 shows the variation of coating thickness as a function of time on AZ91D alloy at constant temperature and pH. The coating thickness was directly proportional to the plating time.

In the present investigation, coating formed in optimised bath composition was found to be amorphous possibly with microcrystalline areas (Fig. 3a). The broad peak in the diffractogram corresponds to the dominant peak for nickel. Although not shown, the X-ray diffraction studies of the deposit formed in bath with TU, MBT and MBT + TU also revealed amorphous/microcrystalline structure. Fig. 3b shows the microstructure of the electroless nickel-coating along the thickness direction. The picture reveals a lamellar structure due to the variation in the composition of phosphorus. The concentration profiling of phosphorus along the thickness of the coating (along the vertical line in Fig. 3b) was carried out using EDX, and shown in Fig. 3c. The phosphorus content showed a sinusoidal variation with average phosphorus content decreasing from interior to exterior. The alternate layers contain high amount of phosphorus with layers in between exhibiting lower values. The average phosphorus content in the deposit was 7–8 wt.% with a hardness value ranging between 650 and 750 VHN depending on the plating parameters.

3.3. Coating nucleation and growth

To understand the nucleation and growth of electroless nickel on electrochemically heterogeneous AZ91D sub-

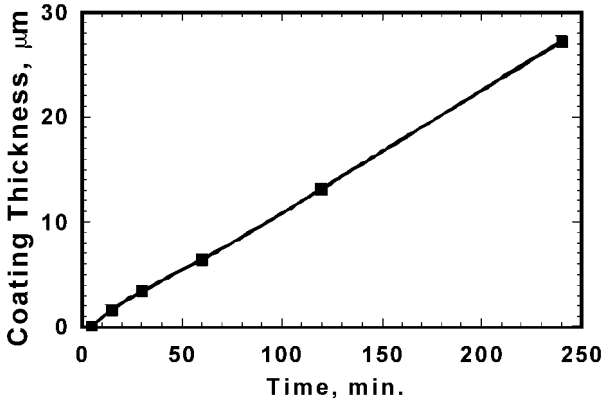

Fig. 2. Electroless nickel-plating rate on AZ91 substrate as a function of time.

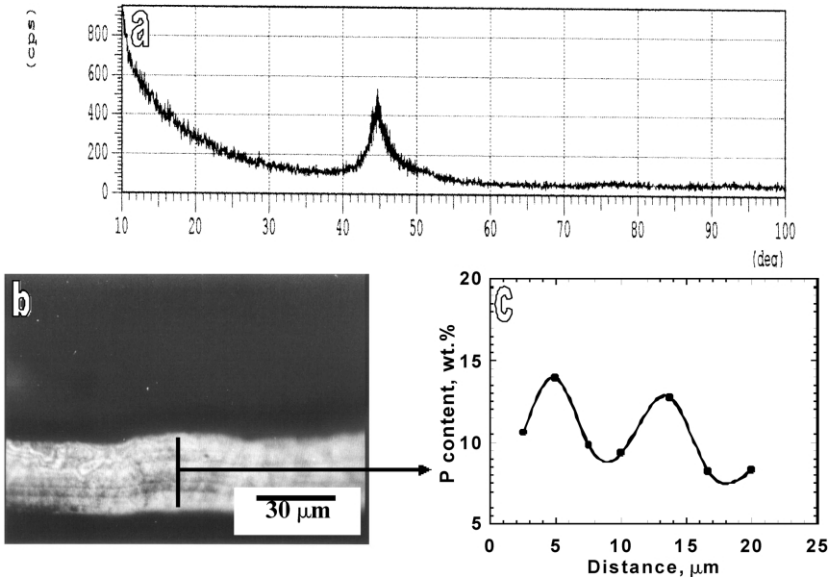

Fig. 3. Structure of electroless nickel-coating on AZ91 substrate after 4 h: (a) diffractogram, (b) cross-section of the coating showing lamellar structure and (c) phosphorus content across the lamellar structure.

strate, plating growth was monitored at very short intervals of time using SEM and EDX. The studies were carried out on substrates after the specified pre-cleaning steps. The effect of various cleaning steps on surface features is shown in Fig. 4. Although the alkaline cleaning did not etch the surface, the surface after chrome–nitric pickling and fluoride activation was etched, so that the different microconstituents could be clearly seen. After hydrofluoric acid cleaning, the surface was found to be smooth and flat (Fig. 4), where flat β phases can be seen as dark phases. The less dark regions adjacent to β-phase is the eutectic α-phase containing a higher amount of aluminium. The etching difference between these phases is due to the difference in aluminium composition as described earlier (Fig. 1b).

Electroless nickel nucleated on the AZ91D substrate at different intervals of time is shown in Fig. 5. The coating has been preferentially nucleated on β-phase, which then spread to eutectic α and primary α-phase. The coating on primary α-phase was formed as a continuation of the deposit on β-phase and eutectic α-phase, after the β-phase and eutectic α-phase was

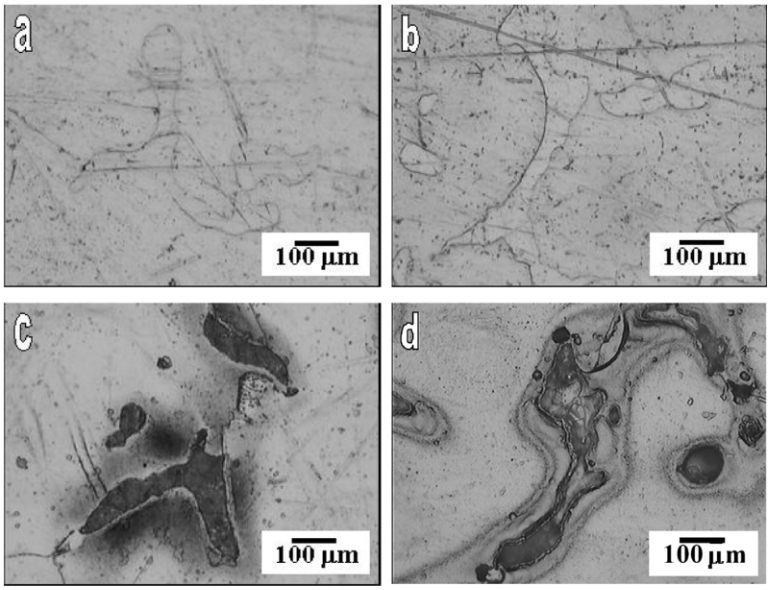

Fig. 4. Effect of pre-cleaning treatment on substrate microstructure: (a) ultrasonic cleaning, (b) alkaline cleaning in 10% NaOH at 60 °C, (c) 6% chromic acid–5% nitric acid pickling and (d) fluoride activation (250 ml 70% HF/l).

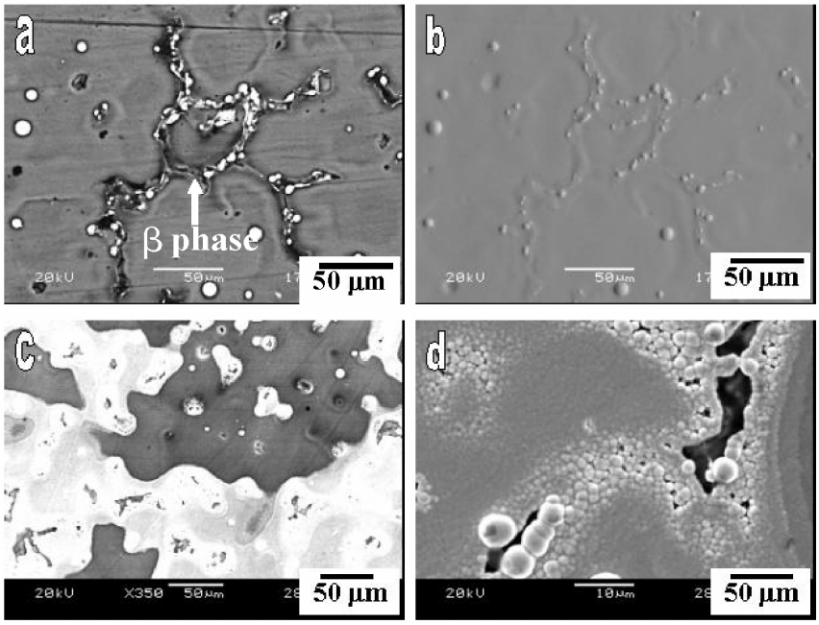

Fig. 5. Early growth of electroless nickel on AZ91 as a function of time: (a) and (b) after 1 min, secondary and topographic mode, respectively; and (c) and (d) after 5 min with (d) at higher magnification showing the morphology of deposit around β-phase.

covered with coating (Fig. 5). However, the coating on the β-phase was discontinuous and grew slowly, which led to a concentration of defects over this region. The EDX analysis of the early stage deposits on β-phase at different intervals of time showed slightly lower amounts of phosphorus content, which increased simultaneously with coating growth. However, this phenomenon was observed in a very thin layer of coating at the surface while on the average, as shown in Fig. 3c, the phosphorus content decreased with coating growth.

Fig. 6 shows the surface morphology of the coating that was attached to the substrate after peeling off from

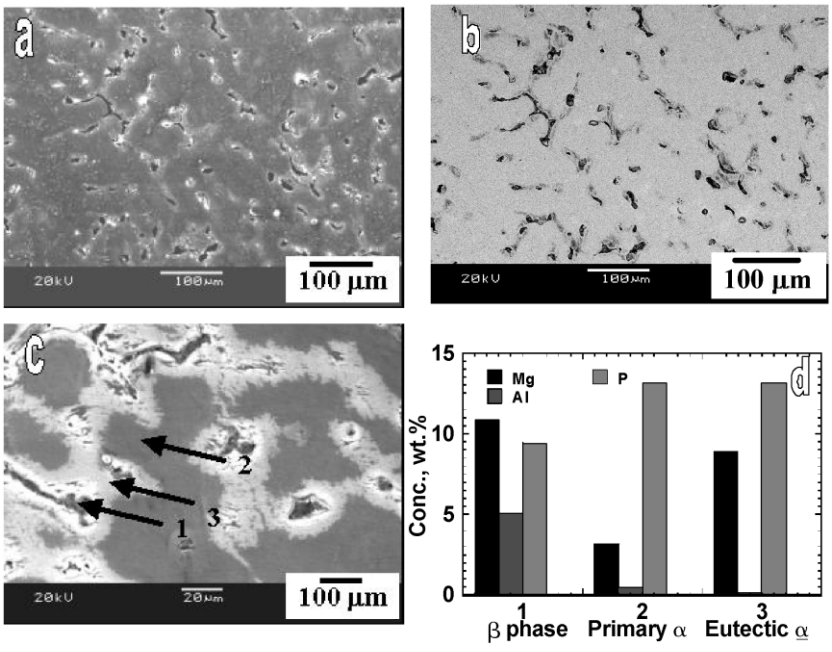

Fig. 6. SEM surface morphology and results of EDX analysis of the coating surface attached to substrate after peeling off: (a) secondary, (b) back scattered, (c) magnified picture showing the morphology near the β-phase and (d) results of EDX analysis at locations 1, 2 and 3 in picture (c).

Table 4
Rate, phosphorus content and hardness of coating with different Ligand–nickel (citric acid/Ni^{2+}) ratio in the coating bath

Citric acid/Ni^{2+} Ratio	Coating rate (μm/h)	Phosphorus content (wt.%)	Hardness (VHN)
0.16	No deposition		
0.33	6.00	7.61	665
0.64	5.41	6.86	651
0.95	No deposition		

the surface. The position marked 1 in the photograph shows the areas of coating attached to β-phase. It can be seen that the coating contained β-phases broken while pulling out. The EDX analysis on the surface of the peeled off coating showed the following results.

EDX analysis at locations 1, 2 and 3 shows a variation of Al, Mg and P content as shown in Fig. 6d. At location 1, the EDX analysis revealed Mg and Al composition corresponding to the β-phase, while the phosphorus content was slightly lower compared to coating areas attached to primary α and eutectic α-phase. Areas of the coating attached to eutectic α-phase showed a higher amount of Mg than the primary α-phase. However, both primary and eutectic α showed very little amount of aluminium. The SEM picture shown in Fig. 6c shows the surface of the substrate material after the coating has been removed from the surface. It can be seen that the β-phase was fractured while pulling out. The fractured surface is visible on the micrographs (marked 1 in the picture). Some corrosion attack is evident on eutectic α-phase (position 2), while the primary α-phase was essentially unattacked (position 3).

3.4. Effect of coating parameters

Both the pre-cleaning steps and the concentration of bath constituents have an influence on electroless nickel-coating. The effect of these bath parameters on the electroless nickel deposition of Mg is not available in the literature. In the present investigation, the effect of complexing agent, fluoride ion concentration, effect of stabilizer concentration such as thiourea and effect of MBT on electroless nickel-plating have been investigated by monitoring coating rate, surface hardness, phosphorus content and surface morphology.

3.4.1. Effect of ligand–nickel ratio

Table 4 gives the coating rate, phosphorus content and hardness of the coating as a function of ligand–nickel ratio. The optimum ratio of ligand–nickel was between 0.33 (Ligand:Ni^{2+} ≅ 1:3) and 0.64 (Ligand:Ni^{2+} ≅ 1:1.5) (i.e. citrate concentration of 5.2–7.8 g/l). Within this range of concentration, the effect of ligand on coating characteristics was found to be similar, although in terms of phosphorus content, the best ligand–nickel ratio was 0.33 (Ligand:Ni^{2+} ≅ 1:3). Above or below this concentration, the coating rate was drastically reduced or inhibited. The surface morphology of the coating did not show significant variation with the change in ligand–nickel ratio.

3.4.2. Effect of fluoride ion concentration

The fluoride ion is an essential component for electroless nickel-plating bath for magnesium, and its presence in the bath was reported to improve adhesion. In the present investigation, ammonium bifluoride was used as the source of fluoride ion. Variation of coating rate, phosphorus content and hardness with concentration of ammonium bifluoride in the coating bath is given in Table 5. The values show that the optimum concentration of ammonium bifluoride in the bath should be approximately 7.5 g/l, although within the concentration range of 7.5–15 g/l, the difference was found to be insignificant. However, the coating produced at 7.5 g/l showed a hardness value of ∼60 VHN higher than the coating produced with 15 g/l of ammonium bifluoride. Fig. 7a and b show the surface topographic pictures of the coatings produced from baths with 0 g/l and 7.5 g/l of ammonium bifluoride, respectively. The deposit formed at 7.5 g/l was found to be more combat and defect free. However, the simple tape-test for adhesion

Table 5
Rate, phosphorus content and hardness of coating with different amounts of ammonium bifluoride in the coating bath

Concentration of Ammonium bifluoride (g/l)	Coating rate (μm/h)	Phosphorus content (wt.%)	Hardness (VHN)
0	1.93	1.93	342
7.5	8.11	8.11	780
15	5.98	5.98	665
22.5	No deposition		

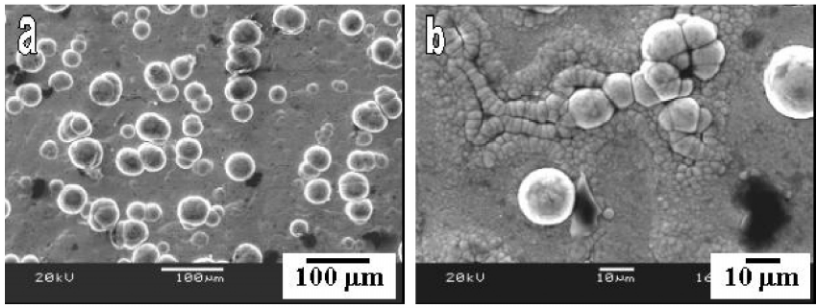

Fig. 7. Effect of ammonium bifluoride on the morphology of the coating on AZ91: (a) 7.5 g/l and (b) without fluoride.

indicated higher adhesion for the coating produced with 15 g/l bifluoride in the bath. Absence of ammonium bifluoride or a concentration above 15 g/l produced very inferior coating (Fig. 7b) or almost inhibited the coating.

3.4.3. Effect of stabilizer (thiourea) concentration

The effect of thiourea concentration on coating rate, phosphorus content and hardness of the coating is given in Table 6. It can be seen that the safe range for thiourea stabiliser is within the range of 0.5–1 mg/l. Within this range, the phosphorus content in the coating remained the same. Below 0.5 mg/l, the bath decomposes spontaneously, correspondingly a higher amount of phosphorus content can be seen in the coating, possibly due to the formation of nickel phosphide. However, above a concentration of 1 mg/l, the coating was totally inhibited.

3.4.4. Effect of MBT on electroless nickel-plating

Heterocyclic organic compounds are widely used as accelerators in electroless plating processes. MBT is one among them, which is found useful in many electroless plating processes. In the present investigation, the effect of MBT was studied with and without the presence of thiourea in the bath. The coating properties as a function of MBT concentration is shown in Fig. 8. Addition of 0.5 mg/l of MBT gave the best deposition with maximum hardness, although the effect was similar in the concentration range of 0.25–0.5 mg/l. However, addition of MBT without thiourea had destabilised the bath in the long run. So it was necessary to optimise the concentration of MBT in the presence of TU. Fig. 9 shows the effect of TU + MBT at different concentrations on coating properties. A concentration of 0.5 mg/l TU + 0.25 mg/l MBT was found to be the optimum value, so that it produced increased coating rate, high phosphorus content and hardness.

4. Discussion

4.1. Early stage growth and coating morphology

Direct plating of magnesium alloys with electroless nickel is still a challenge. Only a limited amount of literature is available [28,29] on the electroless nickel-plating of magnesium alloys and applications. The process is more complicated when the substrate contains second phase particles as for AZ91, which makes the alloy electrochemically heterogeneous. The three microstructural constituents in AZ91 alloy (Fig. 1) namely β, eutectic α and primary α-phase have different electrochemical potentials [10]. This is attributed to the different levels of aluminium in these phases. As shown in Fig. 1b, aluminium concentration typically varies from $\sim$35% in the β-phase to $\sim$12 and $\sim$5 wt.% in the eutectic and primary α-phase, respectively.

Electrochemically β-phase is reported to be more cathodic (more noble) to eutectic α and primary α [10]. Lunder et al. [10] reported that the corrosion potential of β-phase in 5% NaCl saturated with $Mg(OH)_2$ is approximately -1.2 V vs. SCE, whereas the values for pure Mg and AZ91 are -1.66 V and -1.62 V vs. SCE, respectively. The lower aluminium containing primary α-phase is expected to have most active (more negative)

Table 6
Phosphorus content and hardness of coating with different amounts of thiourea in the coating bath

Concentration of thiourea (mg/l)	Coating rate (µm/h)	Phosphorus content in the deposit (wt.%)	Hardness (VHN)
0	8.15	25.00	527
0.5	6.70	8.00	593
1.0	6.77	8.00	620
2.0	1.63	–	–

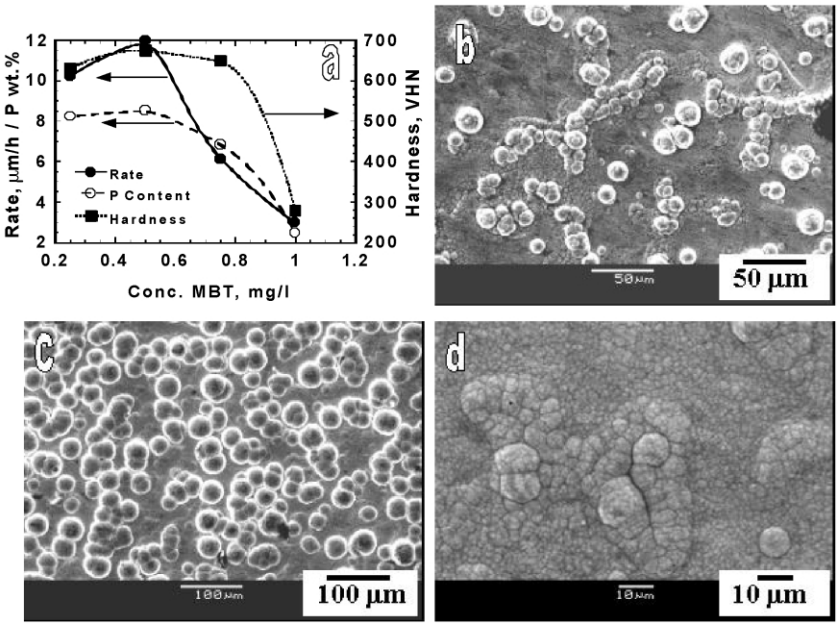

Fig. 8. Effect of MBT on electroless nickel-coating on AZ91: (a) coating rate, phosphorus content and hardness; and typical surface morphology of coating at concentrations (b) 1 mg/l, (c) 0.5 mg/l and (d) 0.75 mg/l.

potential in AZ91 [26]. In such a situation, one would expect preferential nucleation of electroless nickel on the α-phase. However, the present study shows preferential nucleation of nickel deposit on β-phase (Fig. 5). Possible explanation is that the initial stage of deposition has been influenced by a galvanic coupling between β-phase and adjacent eutectic α-phase. The electrons produced by the anodic dissolution of magnesium from the α-phase are consumed by the cathodic deposition of electroless nickel on β-phase. The presence of $Mg(OH)_2$ over eutectic α-phase and less phosphorus in early nickel deposits might support this argument. The above explanation could be represented by the chemical equation as follows:

At the α-phase, magnesium dissolved as Mg^{2+} ions according to the reaction:

$$Mg = Mg^{2+} + 2e^{-} \quad (1)$$

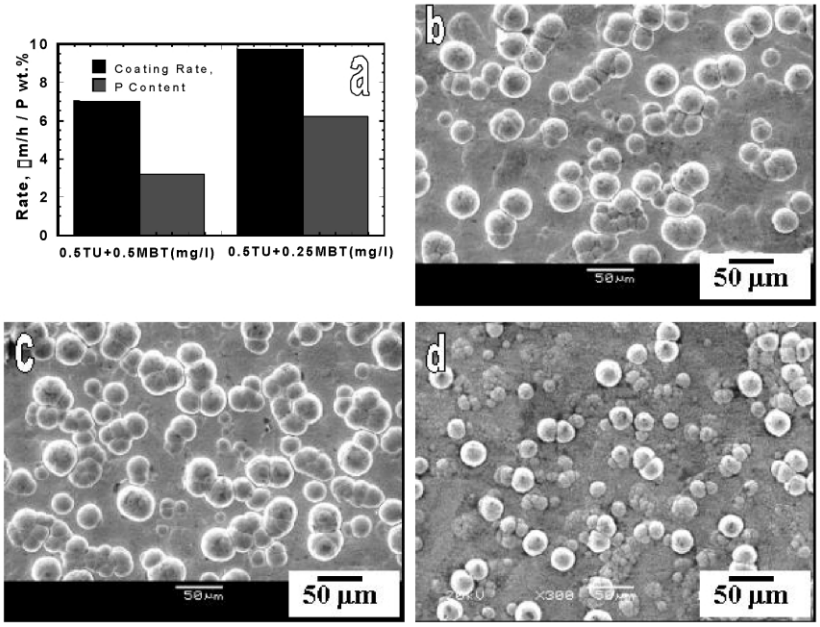

Fig. 9. Effect of MBT + TU on electroless nickel-coating on AZ91: (a) coating rate, phosphorus content and hardness; and surface morphology of coating at concentrations (b) 0.5 mg/l TU + 0.25 mg/l MBT, (c) 0.5 mg/l TU + 0.5 mg/l MBT and (d) 1 mg/l TU.

At the β-phase, the electrons produced from the Eq. (1) are consumed for the reduction of nickel.

$$Ni^{2+} + 2e^- = Ni^o \quad (2)$$

However, more electrochemical evaluation is needed to prove the above mechanism in order to understand the early stage growth behaviour of electroless nickel on AZ91 alloy. Xiang et al. [30] also have reported preferential nucleation of electroless nickel on second phase particles in magnesium alloys during plating, and no phosphorus was found in the initial deposited nickel.

The lamellar structure of the (Fig. 3b) deposit has been attributed to the compositional variation of phosphorus within the deposit as observed in Fig. 3c. The cause of the compositional variation has been explained in terms of periodic fluctuations in the pH of the plating solution adjacent to the deposit surface [31,32]. The overall decrease in phosphorus content with coating thickness might be attributed to the reduction in the concentration of hypophosphite as coating proceeds. The structure of the deposit observed is in agreement with earlier observation that the structure of electroless nickel with 4–7 wt.% phosphorus is generally amorphous [33].

4.2. Effect of bath composition

The nickel source in the present investigation was basic nickel carbonate ($NiCO_3$ $2Ni(OH)_2$ $4H_2O$) and the reducing agent was sodium hypophosphite. Citric acid monohydrate was added as the complexing agent that provides a quadridentate anion for chelation with nickel cation. To activate the magnesium surface, fluoride was added in the form of hydrofluoric acid and ammonium bifluoride, which also increases the adhesion of the coating. The presence of citric acid and ammonium bifluoride also serves the purpose of buffers and accelerators. The pH of the solution was controlled within the range of 7–8 using ammonium hydroxide. The autocatalytic electroless nickel deposition was initiated by catalytic dehydrogenation of the reducing agent with the release of hydride ion, which then supplied electrons for the reduction of nickel ion [27].

Electroless deposited nickel usually contains 3–15 wt.% of co-deposited phosphorus originating from hypophosphite ion. The quantity of phosphorus in the coating determines several engineering properties of electroless nickel.

The role of the complexing agent on electroless nickel-coating on AZ91 alloy can be explained on the basis of three aspects i.e. (a) a reduction in the concentration of free nickel ions, (b) preventing the precipitation of basic nickel salts and nickel phosphate, and (c) exerting a buffering action.

The coating rate on AZ91 alloy increased initially with increase in ligand–nickel ratio upto a ratio of 0.33, above which the rate decreases (Table 4). Several theories have been proposed to explain the variation in coating rate with ligand concentration. De Minjer and Brenner [34] argued that the maximum is the result of the low adsorption of ligand on the catalytic surface at low concentrations, which accelerates the reaction. At higher concentrations, there is a high adsorption of ligand on the surface, which poisons the reaction.

A more plausible explanation suggests that the increase in rate is due to the buffering action of the complexing agents [35]. Maximum rates occur while there are uncoordinated (solvated) sites remaining on the nickel ions, i.e. nickel ions are only partially complexed or chelated. Partially complexed nickel ions retain some of the properties of free, solvated nickel ions. Hence, for ligand concentrations up to values where the maximum plating rates occur, buffering is the dominant function of the various ligands.

An explanation based on pH is inadequate to explain the decrease in rate with further increase in ligand concentration beyond maximum. The pH of the plating bath changes very little with continued plating. Moreover, the buffer capacity of the complexing agent does not parallel the plating rates obtained with them.

However, a decrease in plating rate with increase in ligand concentration (or ligand–nickel ratio), is most likely due to the co-ordination of the remaining solvated sites with ligand atoms [35]. The concentration of free nickel ions decrease and the metal ions take on the characteristics of complexed or chelated nickel ions.

Fluoride ion is an essential component in electroless nickel-plating of magnesium alloys. The initial dip in hydrofluoric acid activates the substrate surface, and forms a fluoride film over the surface. Several researchers studied the reactions between fluoride ion and magnesium [36,37] in relation to corrosion protection. Fluoride ion is reported to be a good corrosion inhibitor for magnesium and its alloys. Further, good corrosion resistance of magnesium base materials in severe environments such as F_2 gas and aqueous and gaseous HF has been reported [36,37]. The protection is due to the formation of a MgF_2 film on the surface of the metal. However, the protective effect in aqueous solutions seems to depend on solution pH and fluoride concentration. As a result, fluorides are constituents of several common anodic coating baths, known as DOW17 and HAE [37–39]. In electroless nickel-plating, formation of magnesium fluoride film over the substrate surface during the pre-cleaning step prevents the oxidation of otherwise reactive magnesium during the transfer of material to plating bath. In the plating bath, the deposition of electroless nickel takes place by replacement of the fluoride film. The presence of fluoride in the bath stabilizes the film on the surface, however, an increase in concentration of fluoride above a value makes the removal of fluoride film for nickel deposition impossible

(Table 5). Xiang et al. [30] have reported that for electroless nickel-plating of magnesium alloys, different fluoride/oxide ratio in the surface film caused different deposition rates.

Although the two heterogeneous partial reactions require a catalytic surface on which to occur, Gutzeit [40,41] found that they could also easily happen on the surfaces of solid particles of colloidal dimensions present in the solution. As the formation of these colloidal particles is uncontrollable and the nickel deposition process is autocatalytic, working electroless nickel baths may decompose spontaneously at any time by triggering a self-accelerating chain reaction on those colloidal particles. So in practice, all working electroless nickel bath contain some kind of stabiliser (catalytic inhibitor) to prevent such spontaneous decomposition. The strong adsorption of stabiliser ions on a catalytic surface block the catalytic sites from being used for the adsorption of reactants, thus impedes the deposition process. When the surface density of adsorbed stabiliser ions reaches a certain level, the deposition process could be completely inhibited (Table 6). As the concentration of stabiliser in bulk solution is usually in the ppm range, unlike the adsorption of reactants, which is kinetically controlled, the adsorption of stabiliser is diffusion limited.

Although complexing agent is essential in electroless nickel-plating baths, its presence sometimes reduces the speed of the plating reaction. To overcome this, accelerators can be added to electroless nickel-plating solution. For AZ91, presence of MBT alone in the bath without thiourea, doubled the plating rate. The presence of MBT and thiourea together in the bath also gave significant increase in plating rate. These accelerators are thought to function by loosening the bond between hydrogen and phosphorus atoms in the hypophosphite molecule, allowing it to be more easily removed and adsorbed on to the substrate surface. The most suitable compounds for this purpose are heterocyclic organic compounds with oxygen or nitrogen atoms as these have a lone pair of electrons to participate in the bonding process. The delocalisation of electrons possible in these molecules makes them suitable to use as accelerators in electroless nickel-plating process. The MBT heterocyclic ring consists of two sulfur and a nitrogen atom. These atoms have lone pairs of electrons to participate in the electroless nickel deposition process.

5. Conclusions

1. The electroless nickel-coating deposited on AZ91D alloy in optimised bath showed amorphous structure with 7 wt.% P and a hardness value of 600–700 VHN. The microstructure of the coating in the transverse direction showed lamellar structure with a phosphorus content varying in a sinusoidal manner.
2. A strong influence of substrate microstructure was found. Initially, the coating was nucleated preferentially on β-phase. The coating spread over to primary α-phase, once the β-phase and eutectic α-phases were covered with electroless nickel.
3. Optimum ligand–nickel ratio was found to be 0.33 (Ligand:$Ni^{2+} \cong 1{:}3$), whereas the best concentration of thiourea was 1 mg/l. Fluoride ions were essential to plate electroless nickel on AZ91D alloy with an optimum concentration of 7.5 g/l of ammonium bifluoride.
4. The presence of 0.5 mg/l of MBT in the plating bath doubled the plating rate. However, for a stable bath, the optimum concentration of thiourea and MBT was 0.5 mg/l of former with 0.25 mg/l of the latter.

References

[1] D. Magers, Magnesium alloys and their applications, in: B.L. Mordike, K.U. Kainer (Eds.), Proceedings of the Conference on Magnesium Alloys and their Applications, Wekstoff-informationsgesellschaft, 1998, p. 105.
[2] S. Schumann, F. Friedrich, (in Ref. D. Magers), Magnesium alloys and their applications, in: B.L. Mordike, K.U. Kainer (Eds.), Proceedings of the Conference on Magnesium Alloys and their Applications, Wekstoff-informationsgesellschaft, 1988, p. 3.
[3] L. Whitby, in: F.L. LaQue, H.R. Copson (Eds.), Corrosion Resistance of Metals and Alloys, 2nd ed, Reinhold, New York, 1963, p. 169.
[4] G.L. Makar, J. Kruger, Int. Mater. Rev. 38 (1993) 138.
[5] G. Song, A. Atrens, M. Dargusch, Corros. Sci. 41 (1999) 249.
[6] O. Khaselev, J. Yahalom, Corros. Sci. 40 (1998) 1149.
[7] D. Daloz, P. Steinmetz, G. Michot, Corrosion 53 (1997) 944.
[8] T.J. Warner, N.A. Thorne, G. Nussbaum, W.M. Stobbs, Surf. Interface Anal. 19 (1992) 386.
[9] F. Hehmann, R.G.J. Edyvean, H. Jones, F. Sommer, in: Proceedings of the International Conference on Powder Metallurgy and Aerospace Materials, Lucerne, Switzerland, November 2–4, 1987, p. 46.
[10] O. Lunder, J.E. Lein, T.Kr. Aune, K. Nisancioglu, Corrosion 45 (1989) 741.
[11] C.F. Chang, S.K. Das, D. Raybould, A. Brown, Met. Powder rep. 41 (1986) 302.
[12] C.F. Chang, S.K. Das, D. Raybould, Rapidly Solidified Materials, American Society for Metals, Metals Park, OH, 1986, pp. 129–135.
[13] M. Bayes, I. Sinitskaya, K. Schell, R. House, T I Met. Finish. 69 (1991) 140.
[14] R.N. Duncan, Plat. Surf. Finish. 83 (1996) 65.
[15] K.L. Lin, J.W. Hwang, Mater. Chem. Phys. 76 (2002) 204.
[16] M.I. Jafar, M. Broadhurst, S.A. Ashton, Br. Corros. J. 31 (1996) 239.
[17] M.A. Sanchez, L.A. Parra, O.A. Perez, O. De Rincon, Corros. Rev. 19 (2001) 105.
[18] G.O. Mallory, J.B. Hajdu (Eds.), Electroless Plating: Fundamentals and Applications, AESF, Florida, 1990, p. 1.
[19] L. Das, D.T. Chin, R.L. Zeller, G.L. Evarts, Plat. Surf. Finish. 82 (1995) 56.
[20] C. Kerr, D. Barker, F.C. Walsh, T I Met. Finish. 74 (1996) 214.

[21] C.G. Fan, J.P. Celis, J.R. Roos, Surf. Coat. Technol. 50 (1992) 289.
[22] G.W. Reade, C. Kerr, B.D. Barker, F.C. Walsh, T I Met. Finish. 76 (1998) 149.
[23] S.W. Court, B.D. Barker, F.C. Walsh, T I Met. Finish. 78 (2000) 157.
[24] A.P. Vangool, P.J. Boden, S.J. Harris, T I Met. Finish. 65 (1987) 108.
[25] C. Kerr, D. Barker, F. Walsh, T I Met. Finish. 75 (1997) 81.
[26] R. Ambat, N.N. Aung, W. Zhou, Corros. Sci. 42 (2000) 1433.
[27] ASM Hand Book, Vol. 5, Surface engineering, electroless nickel-plating, 1994, p. 290.
[28] A.K. Sharma, M.R. Suresh, H. Bhojraj, H. Narayanamurthy, R.P. Sahu, Met. Finish. 96 (1998) 10.
[29] A.K. Sharma, H. Narayanamurthy, H. Bhojaraj, J.Md. Mohideen, Met. Finish. (1993) 34.
[30] Y.H. Xiang, W.B. Hu, X.K. Liu, C.Z. Zhao, W.J. Ding, T I Met. Finish. 79 (2001) 30.
[31] A.W. Goldenstein, W. Rostoker, F. Schlossberger, G. Gutzeit, J. Electrochem. Soc. 104 (1957) 104.
[32] F. Ogburn, C.E. Johnson, Plating 60 (1973) 1043.
[33] N.M. Martyak, S. Wetterer, L. Harrison, M. Mc Neil, R. Heu, A.A. Neiderer, Plat. Surf. Finish. 80 (1993) 60.
[34] C. de Minjer, A. Brenner, Plating 44 (1960) 63.
[35] The electroless nickel-plating bath: effect of variables on the process, in: G.O. Mallory, J.B. Hajdu (Eds.), Electroless Plating: Fundamentals and Applications, AESF, Florida, 1990, p. 57, Chapter 2.
[36] M.R. Bothwell, in: H.P. Godard (Ed.), The Corrosion of Light Metals, John Wiley and Sons, New York, 1967, p. 257.
[37] R.S. Busk, Magnesium Products Design, Marcell Dekker, New York, 1987.
[38] B. Olberts, A.T. Haug, Metalloberflache 43 (1989) 174.
[39] M. Thoma, Metalloberflache 38 (1984) 393.
[40] G. Gutzeit, Plating 46 (1959) 1158.
[41] G. Gutzeit, Plating 47 (1960) 63.